Global Analysis of ICRF Waves and Alfvén Eigenmodes in Toroidal Helical Plasmas

A. Fukuyama, E. Yokota, T. Akutsu

Department of Nuclear Engineering, Kyoto University, Kyoto, Japan

email contact of main author: fukuyamanucleng.kyoto-u.ac.jp

Abstract. The full wave code TASK/WM was extended to analyze the waves in a plasma with three-dimensional inhomogeneity and was applied to the analysis of propagation and absorption of the ICRF waves in the large helical device (LHD). We have studied various parameter dependence of radial power deposition profile and antenna loading impedance; frequency, minority ion density ratio, toroidal mode number. The dependence on the minority ion ratio agrees well with the experimental observation on LHD. The code also has a capability to describe the three kinds of weakly damped Alfvén eigenmodes, GAE, TAE and HAE, in toroidal helical plasmas. We found several kinds of eigenmodes and studied their behavior.

1. Introduction

Global analysis of the ion cyclotron range of frequency (ICRF) waves has been successfully applied to study heating and current drive in axisymmetric tokamak plasmas [1-5]. In toroidal helical devices, such as stellarator and torsatron/heliotron, however, the global analysis of ICRF waves was limited to a linear helical system [6]. We have revised the full wave code TASK/WM to deal with the plasma with three-dimensional inhomogeneity and applied to the analysis of propagation and absorption of the ICRF waves in the large helical device (LHD).

2. Full Wave Code

In the TASK/WM code, we solve Maxwell's equation for wave electric field $\vec{E}$ with complex frequency ω,

$$\vec{\nabla} \times \vec{\nabla} \times \vec{E} = \frac{\omega^2}{c^2} \overleftrightarrow{\epsilon} \cdot \vec{E} + \mathrm{i}\,\omega\mu_0 \vec{j}_{\mathrm{ext}} \tag{1}$$

as a boundary value problem based on the three-dimensional formulation [7]. The external current $\vec{j}_{\mathrm{ext}}$ in the right hand side denotes the antenna current in ICRF heating and vanishes for eigenmodes. Taking account of the real geometry of the plasma, we employ the non-orthogonal flux coordinates (ψ, θ, ϕ) calculated by the magnetohydrodynamic equilibrium code, VMEC [8].

The response of the plasma is expressed by a dielectric tensor including kinetic effects. The wave electric field is expressed as a sum of the Fourier components with poloidal mode numbers m and toroidal mode numbers n,

$$\vec{E}(\psi, \theta, \phi) = \sum_{mn} \vec{E}_{mn}(\psi) e^{\mathrm{i}(m\theta + n\phi)}. \tag{2}$$

These components are coupled with each other through the inhomogeneity of the plasma. The parallel wave number essential for the wave-particle interaction can be accurately

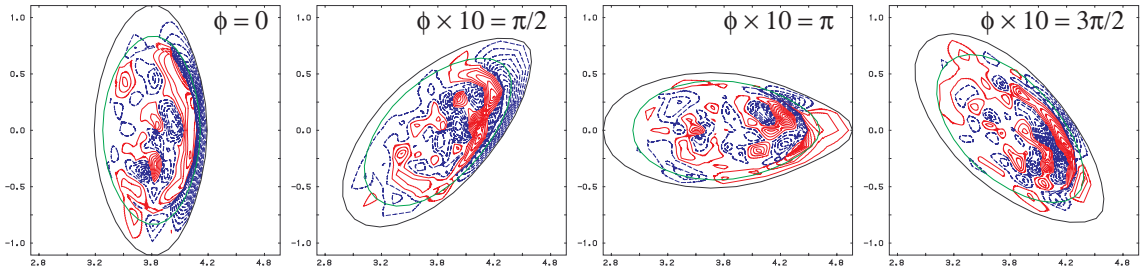

FIG. 1. Contour of the poloidal component of the wave electric field on the poloidal cross sections at four different toroidal angles.

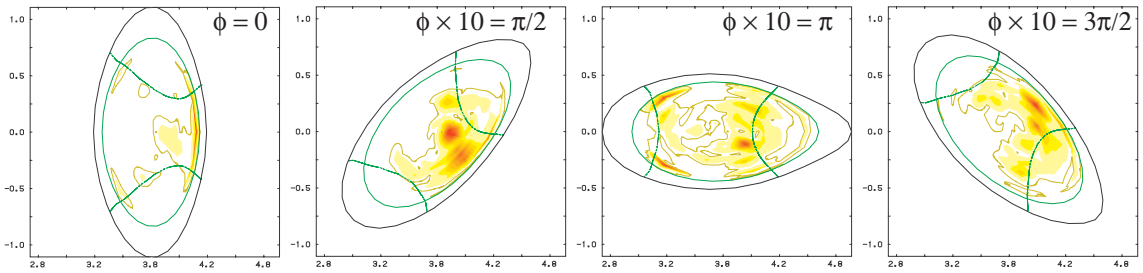

FIG. 2. Intensity plot of the power density absorbed by the minority ions. The dashed line indicates the cyclotron resonance surface of the minority ions

specified by m and n. Although the dielectric tensor may include the wave-particle interaction along the field line and the finite gyroradius effect, we employ the cold plasma approximation with collisional damping ($\nu/\omega = 0.03$) in this paper and elucidate the three-dimensional effects.

3. Analysis of ICRF Wave Heating

We have analyzed the case of fast wave minority heating (He+H) in a LHD-grade plasma: $N = 10$, $L = 2$, $B_0 = 3\,\mathrm{T}$, $R_0 = 3.8\,\mathrm{m}$, $n_{\mathrm{e0}} = 3 \times 10^{19}\,\mathrm{m}^{-3}$, $n_{\mathrm{H}}/(n_{\mathrm{He}} + n_{\mathrm{H}}) = 23.5\%$, $f = 42\,\mathrm{MHz}$ and dominant toroidal mode number $n_{\phi 0} = 20$. In most of the following calculations, 3 toroidal modes ($n = n_{\phi 0}$, $n_{\phi 0} \pm 10$) and 15 poloidal modes (m = -7 to 7) are taken into account; we name it 4×16 modes calculation including the zero-amplitude highest modes. The number of radial mesh points is typically 100.

FIG. 1 illustrates the structure of the wave electric field ($\mathrm{Im}E_\theta$) on the poloidal cross sections at four different toroidal angles, $\phi \times 10 = 0$, $\pi/2$, π and $3\pi/2$. The half-turn antenna is located between the plasma and the wall outside of the torus (right hand side in FIG. 1) at $\phi = 0$. The wave electric field has the largest amplitude in the vacuum region near the antenna and penetrate into plasma without focusing.

The profile of power density absorbed by the minority ions is shown in FIG. 2. In front of the antenna ($\phi = 0$), coupling to the slow wave causes localized absorption in a low density surface region. Away from the antenna, however, bulk plasma heating occurs near the two-ion hybrid resonance layer, high field side of the cyclotron resonance layer. Since the location of the cyclotron resonance surface depends on the toroidal angle, three-dimensional analysis is required for quantitative estimates of the deposition profile.

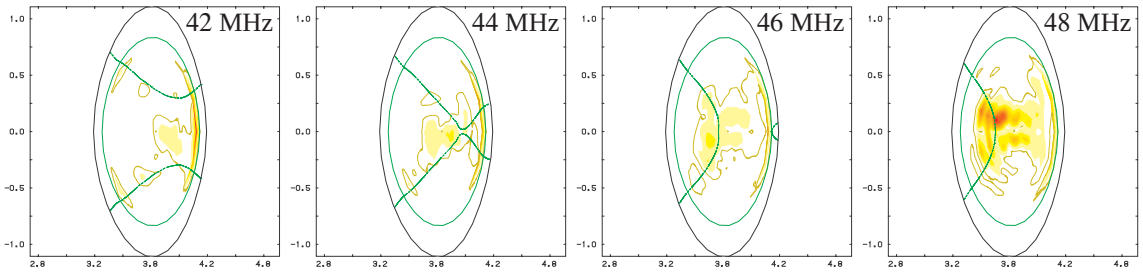

FIG. 3. Frequency dependence of the power deposition profile on the poloidal cross section.

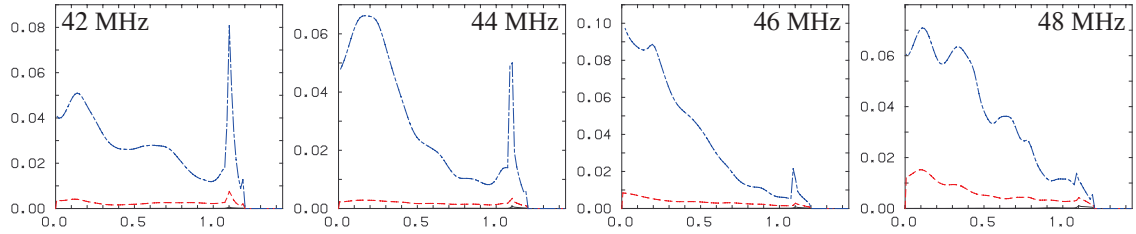

FIG. 4. Frequency dependence of the radial deposition profile. The dashed and dotted lines indicate the power absorbed by minority ions, while the dashed lines collisional power absorption by majority ions.

The dependence on the wave frequency is presented in FIGS. 3 to 5. Deposition profile on the poloidal crosssection ($\phi = 0$) shown in FIG. 3 moves toward the inside of the torus, as the wave frequency increases. The radial distribution in FIG. 4 also indicates the decrease of surface heating and the increase of core heating. Good and stable coupling is obtained between 38 MHz and 48 MHz. Since the cyclotron resonance layer lies near the plasma edge for frequency less than 38 MHz, the deposition profile becomes hollow. Above 48 MHz, the cyclotron layer approaches the high field side plasma edge and the damping becomes weak. Therefore the cavity resonance causes the sensitive behavior of the total power absorption, i.e., antenna loading resistance, as show in FIG. 5.

The total absorption power also depends on the ratio of the ion densities, $n_{\mathrm{H}}/(n_{\mathrm{He}} + n_{\mathrm{H}})$. FIG. 6 shows that the minority heating becomes dominant for minority ion ratio more than 8 %. When the ratio is small, edge heating is substantial and the deposition profile becomes hollow. The optimum ratio is between 10% to 20% for this frequency, f =

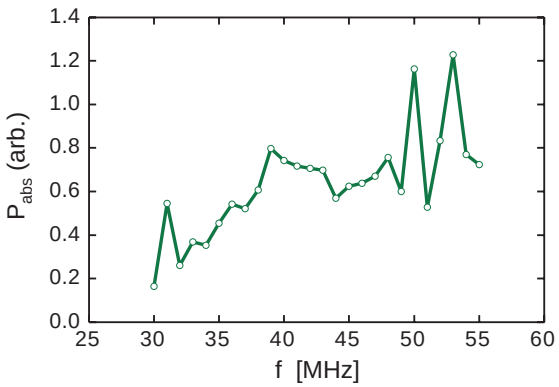

FIG. 5. Frequency dependence of the total power absorption.

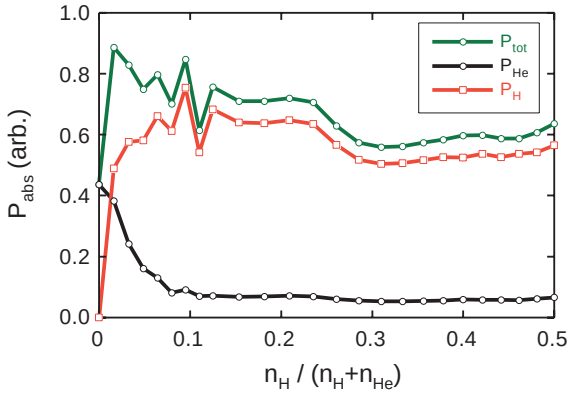

FIG. 6. Dependence of total absorption power on the minority ion ratio, $n_{\rm H}/(n_{\rm He}+n_{\rm n})$. The solid line indicates the total abortion power, the thin line the power absorbed by minority ion and the dashed line by majority ions

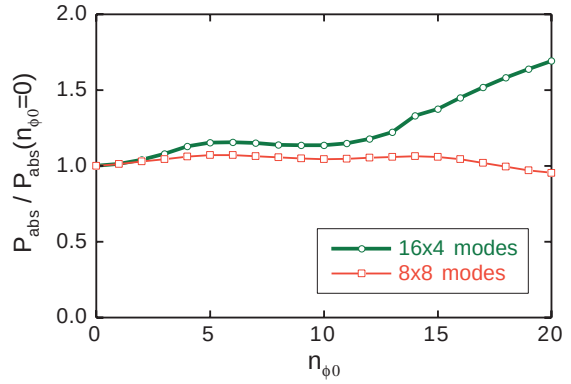

FIG. 7. Dependence of the total absorption power on the central value of the toroidal mode number, $n_{\phi 0}$. The solid line indicates the calculation with 8×8 modes, the thin line 16×4 modes, where $m\times n$ implies poloidal mode number m and toroidal mode number n.

42 MHz. This result agree with the ICRF experiment on LHD [9].

Finally we show the dependence on the toroidal mode number. In a toroidal helical plasmas, the toroidal mode of n couples with the modes of $n_{\pm}N_{\rm h}$, where $N_{\rm h}$ is a toroidal pitch of the helical coil, $N_{\rm h}=10$ for LHD. Therefore the toroidal modes belong to 10 classes and the modes are coupled within the class. Since the number of coupled toroidal modes is limited in a numerical calculation, the result depends on the selection of the toroidal modes. FIG. 7 indicates that the dependence on the toroidal mode number is rather weak and the variation is less than 5% for 8 toroidal modes (from $n_{\phi 0}-30$ to $n_{\phi 0}+30$).

4. Analysis of Alfvén Eigenmode

There are three kinds of weakly damped Alfvén eigenmodes in a toroidal helical plasma; the global Alfvén eigenmode (GAE), the toroidicity-induced Alfvén eigenmode (TAE) and helicity-induced Alfvén eigenmode (HAE). Their characteristics and resonance conditions are given by

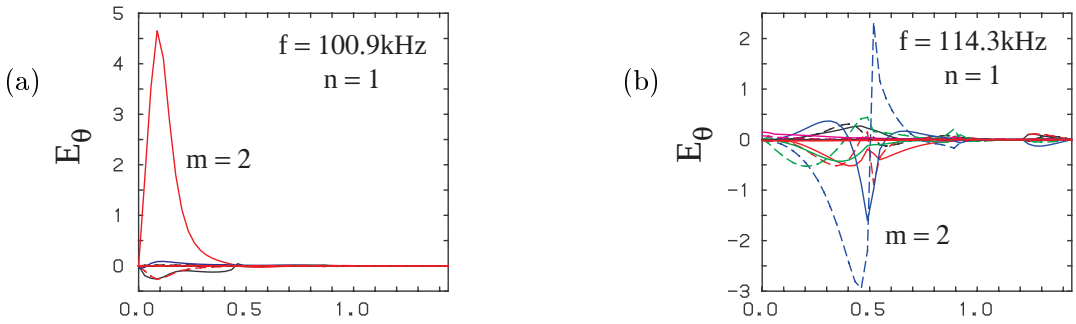

FIG. 8. Typical examples of (a) GAE and (b) electrostatic AE.

GAE: single n, single m, on axis or reversed shear
TAE: single n, multi m, poloidal mode coupling$(m, m+\ell)$,
$$k_{\|} = \ell/2qR, \quad q = -(m+\ell/2)/n$$
HAE: multi n, multi m, toroidal mode coupling $(n, n+N_{\rm h}k)$
$$k_{\|} = (\ell + N_{\rm h}kq)/2qR, \quad q = -(m+\ell/2)/(n+N_{\rm h}k/2)$$

where q is the safety factor. The kinetic and electrostatic Alfvén eigenmodes can exists. The TASK/WM code can describe these modes and calculate the damping rate. FIG. 8 shows (a) a typical GAE mode with $q(0) = -2.3$ and (b) an electrostatic Alfvén eigenmode which localizes near $q = 2$ surface.

5. Discussion

We have demonstrated the capability of the three-dimensional full wave code and have studied the characteristics of ICRF heating in LHD within the cold plasma model. Kinetic analysis which has been applied to the tokamak plasma will be extended to the toroidal helical plasma in near future. Experimental observation of Alfvén eigenmode has been reported in CHS and LHD [10]. Comparison with experimental results is now in preparation.

[1] FUKUYAMA, A., ITOH, K., ITOH, S.-I., Comp. Phys. Rep. **4** (1986) 137.
[2] VILLARD, L., APPERT, K., GRUBER, R., VACLAVIK, J., Comp. Phys. Rep. **4** (1986) 95.
[3] JAEGER, E.F., BATCHELOR, D.B., CARTER, M.D., WEITZNER, H., Nucl. Fusion **30** (1990) 505.
[4] JAUN, A., APPERT, K., VACLAVIK, J., VILLARD, L., Comp. Phys. Comm. **92** (1995) 153.
[5] BRAMBILLA, M., Plasma Phys. Control. Fusion **41** (1999) 1.
[6] FUKUYAMA, A., OKAZAKI, N., GOTO, A., ITOH, S.-I., ITOH, K., Nucl. Fusion, **26** (1986) 151.
[7] VDOVIN, V., WATARI, T., FUKUYAMA, A., Proc. of 1996 Int. Conf. on Plasma Phyis., Nagoya (1997) 1070.
[8] HIRSHMAN, S.P., WHITSON, J.C., Phys. of Fluids **26** (1983) 3553.
[9] KUMAZAWA, R. et al., Proc. of 10th Int. Toki Conf. on Plasma Phys. Control. Nucl. Fusion (January, 1999) VIII-2.
[10] TOI, K., et al., Nucl. Fusion **40** (2000) 1349.